# Nonlinear Effects Mitigation in Coherent Optical OFDM System in Presence of High Peak Power

Yanir London and Dan Sadot

***Abstract*—The nonlinear effects of Mach–Zehnder modulator (MZM) and self phase modulation (SPM), in optical orthogonal frequency division multiplexing (OFDM) under the presence of high peak power is studied. A full coherent optical communication system is presented and analyzed. Standard method to reduce the peak to average power ratio (PAPR) values combined with improved technique to mitigate the nonlinear effect, by means of optimized digital pre-distortion, is analyzed and a full performance analysis is presented.**

***Index Terms*—Nonlinear optics, optical fiber communication, optical modulation, peak to average power ratio.**

## I. Introduction

OPTICAL OFDM is considered to be a promising transmission format, mainly due to its high spectral efficiency and inherent dynamic bandwidth capabilities [1], [2], for the forthcoming 400-Gb/s transmission data rates and above. However, OFDM has a major disadvantage—high peaks power, which in turn results in nonlinear effects, e.g., SPM and MZM nonlinearity.

In the wireless communication field, many methods offer to reduce the PAPR values of the OFDM symbols, and increase the system performance. Han and Lee reviewed the main techniques to reduce PAPR [3]. Goebel *et al.* showed that those techniques can be adopted in optical OFDM systems [4].

Another approach for improving system performance in presence of high peak power is increasing the immunity of the system components and reducing the nonlinear sensitivity. The main nonlinear sensitive components in optical communication systems are the fiber and the optical modulator.

For a single-carrier transmission, high power signal propagating through the fiber can lead to SPM. Lowery used an optimized nonlinearity pre- and post-compensation to improve the received signal quality [5], while Liu and Tkash proposed a joint SPM compensation for 112-Gbps OFDM system [6].

For the MZM components, Killey *et al.* presented a digital MZM pre-distortion to compensate for fiber dispersion in 10-Gp/s NRZ system [7], while Weber *et al.* used electronic pre-distortion to reduce intra-channel nonlinear effects in single-channel 40-Gb/s NRZ transmission system consisting of 100% dispersion compensated spans [8]. In addition, Tang *et al.* proposed a combination of MZM pre-distortion and clipping for Coherent optical OFDM (CO-OFDM) [9].

In this works, in order to mitigate these nonlinear effects, we propose and analyze an optimized digital MZM pre-distortion technique for CO-OFDM system. In addition, the proposed technique is compared with selective mapping (SLM), a standard PAPR reduction technique. We show that both methods are efficient for nonlinearity mitigation, and can be used for optimized system design.

Manuscript received May 03, 2011; revised July 19, 2011; accepted August 18, 2011. Date of publication September 12, 2011; date of current version October 19, 2011. This work was supported in part by the Israeli Science Foundation (ISF) under Contract 322/04.

The authors are with the Department of Electrical Engineering, Ben-Gurion University of the Negev, Beer-Sheva, 84105, Israel (e-mail: yanirl@bgu.ac.il).

Color versions of one or more of the figures in this paper are available online at http://ieeexplore.ieee.org.

Digital Object Identifier 10.1109/JLT.2011.2167715

## II. Background

The basic approach of OFDM is to group together a series of messages where each message is carried by a different tone at a reduced data rate. Each one of the tones is orthogonal to the others, thus the OFDM signal has high spectral efficiency [1]. In addition, due to the orthogonality feature, each tone can be independently added or dropped without affecting the rest of the signal constellation, thus enabling dynamic bandwidth manipulation.

The zero padded frequency domain digital data can be defined as [10]:

$$\tilde{\mathbf{X}} = [X_0, \ldots, X_{N/2-1}, \underbrace{0, \ldots, 0}_{N(L-1)}, X_{N/2}, \ldots X_{N-1}] \quad (1)$$

where $X_0, X_1, \ldots, X_{N-1}$ represent the frequency domain useful data at the input of the OFDM transmitter, $N$ is the number of OFDM tones and $L$ is the oversampling factor and a positive integer number that is equal to or larger than 1. The "L-times oversampled" complex envelope of OFDM signal can be expressed as [3]:

$$x_n = \frac{1}{\sqrt{N}} \sum_{l=0}^{N \cdot L-1} \tilde{X}_l \cdot e^{j(\frac{2\pi}{N \cdot L})l \cdot n}, \quad (2)$$

where $\tilde{X}_l$ is a frequency domain data symbols, $l$ is discrete frequency, $n = 0, 1, 2, \ldots, N \cdot L-1$ is discrete time, and $j = \sqrt{-1}$.

Although the OFDM signal is very attractive due to its clear spectral efficiency advantage, it has a major disadvantage as a multi-tone signal: high PAPR values. The PAPR as computed from the L-times oversampled time domain signal is [3]:

$$\mathrm{PAPR} = \frac{\max\limits_{0 \le n \le \mathrm{N} \cdot \mathrm{L}-1} |x_n|^2}{E[|x_n|^2]}, \quad (3)$$

where $E[\cdot]$ denotes the expectation value. It is shown in [11] that $L = 4$ can provide sufficiently accurate PAPR results.

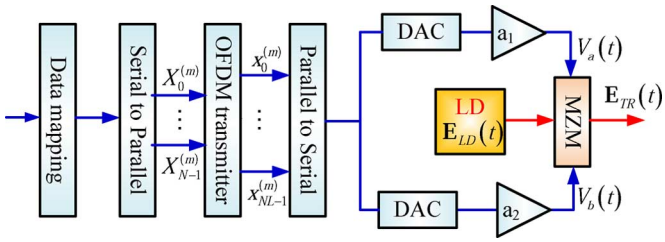


Fig. 1. Standard CO-OFDM transmitter.

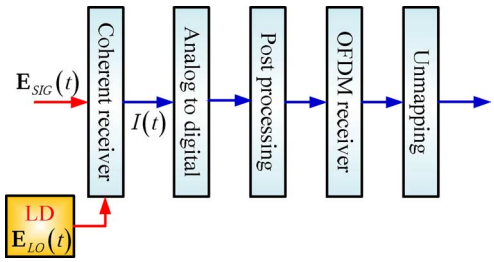


Fig. 2. Standard CO-OFDM receiver.

The high peak signal values may significantly reduce the system performance as being distorted by the nonlinear components. Moreover, PAPR values are random, and depend on the transmitted data.

## III. CO-OFDM System Model

### A. Standard CO-OFDM System

In Figs. 1 and 2 standard CO-OFDM transmitter and receiver are presented [2]. The following analysis is limited to real OFDM signal. This is done for the sake of simplicity, only. However this analysis can be easily extended to include complex signals by using dual-MZM at the transmitter. To generate real OFDM symbols, the following Fourier property, i.e., Hermettian symmetry, needs to be applied:

$$\begin{aligned} X_l^{(m)} &= \left(X_{N-l}^{(m)}\right)^*, \quad l \in \{1, N/2-1\} \\ X_0^{(m)} &= X_{N/2}^{(m)} = C^{(m)} \end{aligned} \tag{4}$$

where $C^{(m)}$ is a real number, $X_l^{(m)}$ is the $l$th frequency domain digital data of the $m$th OFDM symbol while $m$ is a positive integer. In common practice $C^{(m)} = 0$ as it permits DC coupling. The $n$th output of the OFDM transmitter block of the $m$th OFDM symbol is designated as $x_n^{(m)}$.

The applied MZM voltages, $V_a(t)$ and $V_b(t)$ can be expressed by

$$\begin{cases} V_a(t) = a_1 \cdot \sum_{m=1}^{\infty} \sum_{n=0}^{NL-1} x_n^{(m)} \cdot g(t - n \cdot T_S/L - m \cdot N \cdot T_S/L) \\ V_b(t) = a_2 \cdot \sum_{m=1}^{\infty} \sum_{n=0}^{NL-1} x_n^{(m)} \cdot g(t - n \cdot T_S/L - m \cdot N \cdot T_S/L) \end{cases} \tag{5}$$

where $a_1$ and $a_2$ are multiplicative factor, $T_s$ is the mapped symbol duration, e.g., QAM symbol, and $g(t)$ is a zero order hold (ZOH) shaping pulse of a digital to analog converter (DAC), which can be written as

$$g(t) = \begin{cases} 1, & 0 \le t \le T_S \\ 0, & \text{else} \end{cases} \tag{6}$$

It should be noted that different tones may be modulated with different mapping schemes.

The applied voltages to the MZM $V_a(t)$ and $V_b(t)$ modulate the optical field of the laser carrier $\mathbf{E}_{\mathrm{LD}}(t)$ (at null intensity bias) resulting in

$$\mathbf{E}_{\mathrm{TR}}(t) = \mathrm{T}_{\mathrm{MZM}}[V_a(t), V_b(t)] \cdot \mathbf{E}_{\mathrm{LD}}(t), \tag{7}$$

where $\mathrm{T}_{\mathrm{MZM}}[\cdot]$ is the MZM transfer function, which is discussed in more details in Section III-B. $\mathbf{E}_{\mathrm{LD}}(t)$ is given by

$$\mathbf{E}_{\mathrm{LD}}(t) = \sqrt{\frac{P_{\mathrm{LD}}}{2}} \cdot e^{-j(\omega_{\mathrm{LD}}(t) \cdot t + \phi_{\mathrm{LD}}(t))} \tag{8}$$

where $P_{\mathrm{LD}}$ is the output power of the optical laser diode, $\omega_{\mathrm{LD}}(t)$ is the instantaneous angular frequency, and $\phi_{\mathrm{LD}}(t)$ is the instantaneous laser phase.

Following propagation through the fiber, the optical signal at the coherent receiver input is given by

$$\mathbf{E}_{\mathrm{SIG}}(t) = \mathrm{T}_{\mathrm{fiber}}[\mathbf{E}_{\mathrm{TR}}(t)], \tag{9}$$

where $\mathrm{T}_{\mathrm{fiber}}[\cdot]$ is a nonlinear operator, described by the Schrödinger equation [12]. In general, there is no analytical solution to (9), especially at the presence of high launched power. Hence, a numerical solution of (9) is executed with the help of the split-step Fourier Transform method [12].

The coherent receiver down-converts the optical signal to the following in-phase and quadrature current signals $I_I(t)$ and $I_Q(t)$, respectively [13], [14]:

$$\begin{cases} I_I(t) = \mathrm{LPF}\left(2R \cdot \mathrm{Re}\left\{\mathbf{E}_{\mathrm{SIG}}(t) \cdot (\mathbf{E}_{\mathrm{LO}}(t))^*\right\}\right) \\ I_Q(t) = \mathrm{LPF}\left(2R \cdot \mathrm{Im}\left\{\mathbf{E}_{\mathrm{SIG}}(t) \cdot \left(\mathbf{E}_{\mathrm{LO}}(t) \cdot e^{-j \cdot \pi/2}\right)^*\right\}\right) \end{cases} \tag{10}$$

where $R$ is the photodiode responsivity, $\mathrm{LPF}(\cdot)$ refers to a low-pass filter operation, $\mathrm{Re}\{\cdot\}$ and $\mathrm{Im}\{\cdot\}$ refer to the real and imaginary components, respectively; $(\cdot)^*$ designates conjugate signal, and $\mathbf{E}_{\mathrm{LO}}(t)$ is the local oscillator laser at the receiver defined as

$$\mathbf{E}_{\mathrm{LO}}(t) = \sqrt{\frac{P_{\mathrm{LD}}}{2}} \cdot e^{-j \cdot (\omega_{\mathrm{LO}}(t) \cdot t + \phi_{\mathrm{LO}}(t))}, \tag{11}$$

In (11) $\omega_{\mathrm{LO}}(t)$ is the instantaneous angular frequency of the laser and $\phi_{\mathrm{LO}}(t)$ is the instantaneous laser phase.

At the coherent receiver output $I_I(t)$ and $I_Q(t)$ are sampled by an analog to digital convertor (ADC) and, in turn, all the channel impairments (e.g., laser and fiber) are removed using recently develop coherent algorithms [5], [15], [16]. Finally, the OFDM symbols can be extracted from the resulting signal.

### B. MZM in Presence of High Peak Power

A high data rate optical system using chirp-free signal usually requires an external modulator. In the analyzed CO-OFDM system, MZM is used.

MZM is a waveguide-based modulator [17], and its output optical field is given by

$$\mathbf{E}_{\text{out}} = \left(\frac{1}{2}e^{j\frac{\pi V_a}{2V_\pi}} + \frac{\gamma}{2}e^{j\frac{\pi V_b}{2V_\pi}}\right)\cdot \mathbf{E}_{\text{in}} \tag{12}$$

where $\mathbf{E}_{\text{in}}$ is the input optical field; $V_a$ and $V_b$ are the data related applied electrical voltages; $V_\pi$ is the electrical voltage that introduces a phase shift of 180° to the optical field; and $|\gamma| \in [0,1]$ is the imperfectness MZM parameter, caused by imbalance between MZM arms length. Since $\gamma = a \cdot e^{j\phi}$, it can be pre-composed for phase modulation such as QAM. In (12) it is assumed that the MZM bandwidth is wider than the analog bandwidth of the transmitted OFDM signal.

In the case of a differential input data in a push-pull configuration $(a_1 = (-a_2) = 1)$ and assuming $\gamma = 1$, the output optical field can be represented by a cosine dependency

$$\mathbf{E}_{\text{out}} = \cos\left(\frac{\pi V_a}{2V_\pi}\right)\mathbf{E}_{\text{in}}. \tag{13}$$

While OFDM signal is applied to modulate $\mathbf{E}_{\text{in}}$ using MZM, distortions may occur at $\mathbf{E}_{\text{out}}$ following the cosine behavior of (13), resulting in a rapid increase in bit error rate at the receiver.

A similar approach to the one shown by Bohara and Ting for power amplifier [18] can be adopted for optical OFDM systems using MZM. The baseband equivalent polynomial model for the output electrical field of the MZM, as described in (13), assuming $\phi_{\text{BIAS}} = 3\pi/2$, is given as

$$y_n = \sum_{k=1}^{K} \alpha_k \cdot (x_n)^k, \quad k-\text{odd} \tag{14}$$

where $x_n$ and $y_n$ are the discrete vectors of applied voltage and MZM output, respectively. $n$ is the discrete time domain samples, $k$ is the order of nonlinearity, and $\alpha_k$ is the nonlinear odd coefficients.

It can be presumed that $X_l$ are i.i.d. random variables with zero mean and variance of $P$ [18]. By the central limit theorem (CLT) [19], when $N$ is large, $x_n$ can be assumed to be a Gaussian process with zero mean and variance $P_{\text{av}} = P/N$ [20].

If the operating region of the MZM is $3V_\pi \pm V_\pi$ (i.e., at the null intensity bias point) a good approximation of the MZM output signal is a third order polynomial, thus (14) is simplified to

$$y_n = \alpha_1 \cdot x_n + \alpha_3 \cdot (x_n)^3. \tag{15}$$

Assuming a linear channel with additive white Gaussian noise (AWGN), the detected signal after ideal channel compensation and after performing discrete Fourier transform (DFT) at the receiver side, is

$$\hat{a}_l = \sum_{n=0}^{N-1} y_n \cdot e^{-j(2\pi/N)l\cdot n} + n_{0,l} \tag{16}$$

where $\hat{a}_l$ is the recovered symbol at the $l$th tone, and $n_{0,l}$ is the AWGN noise with variance $N_0$. After substituting (15) in (16), and some manipulation [18], we obtained

$$\hat{a}_l = a_k \cdot \mu + \eta + n_{0,l} \tag{17}$$

where the multiplicative term are defined as

$$\mu = \alpha_1 + \frac{\alpha_3}{N}\sum_{n=0}^{N-1}\gamma_n \tag{18}$$

and the nonlinear noise components are defined as

$$\eta = \frac{\alpha_3}{N}\sum_{p=0,p\neq k}^{N-1} a_p \left[\sum_{n=0}^{N-1}\gamma_n \cdot e^{j2\pi\cdot \mathrm{n}(-k+p)/N}\right] \tag{19}$$

where $\gamma_n = |x_n|^2$. Thus, each received symbol contains a multiplicative term corresponding to $\mu$, a nonlinear noise component corresponding to $\eta$, and an AWGN term.

The variance of the nonlinear noise is given by [18]

$$\sigma_{\text{NL}}^2 = E[|\eta|^2] = \frac{(\alpha_3)^2 \cdot P^3}{N^3}\left(\frac{3N^2 - 11N + 12}{N}\right). \tag{20}$$

Using (20), the signal to noise ratio (SNR) for each tone is

$$\text{SNR} = \frac{P\cdot\mu^2}{\sigma_{\text{NL}}^2 + N_0}. \tag{21}$$

As seen in (21), the SNR at the receiver after DFT depends upon the coefficients $\alpha_1$ and $\alpha_3$, as well as the power of OFDM symbol, $P_{\text{av}} = P/N$.

Using (21), the BER for the M-ary QAM system at the output of the demodulator [21] is

$$P_b = \frac{1}{\log_2\sqrt{M}}\sum_{k=1}^{\log_2\sqrt{M}} P_b(k), \tag{22}$$

where

$$P_b(k) = \frac{1}{\sqrt{M}}\sum_{i=0}^{(1-2^{-k})\sqrt{M}-1} \times \left\{\begin{array}{l}(-1)^{\lfloor 2^{k-1}i/\sqrt{M}\rfloor}\cdot\left(2^{k-1} - \left\lfloor\frac{i\cdot 2^{k-1}}{\sqrt{M}} + \frac{1}{2}\right\rfloor\right) \\ \cdot \text{erfc}\left((2i+1)\sqrt{\frac{3\log_2 M\cdot\text{SNR}}{2(M-1)}}\right)\end{array}\right\}. \tag{23}$$

### C. Selective Mapping Technique

Various techniques to reduced PAPR values are proposed and used in wireless system [3]. SLM technique, based on electronic implementation with a low data rate loss [22], is one of the extensively used PAPR reduction techniques.

In the SLM technique the data block with the lowest PAPR value from a set of different data blocks, all representing the same information, is selected to be transmitted, and the original information is recovered at the receiver. The block diagram of the SLM technique is shown in Figs. 3 and 4. In the SLM technique, the $m$th frequency domain digital signal $\tilde{\mathbf{X}}^{(m)}$ is cloned $\varepsilon$ times, $\varepsilon$ being the SLM order.

The SLM block has a constant set of $\varepsilon$ different $v$ vectors, each of length $N \cdot L$, which can be written as $\mathbf{v}_u = [v_{u,0}, v_{u,1}, \ldots, v_{u,N\cdot L-1}], u = 1,2,\ldots,\varepsilon$ with $\mathbf{v}_1 = [1,1,\ldots,1]$. The form of $\mathbf{v}_u$ is $v_{u,l} = e^{j\alpha}$, where $l = 0,1,\ldots,N\cdot L-1$ and usually $\alpha = \{0,\pi\}$.

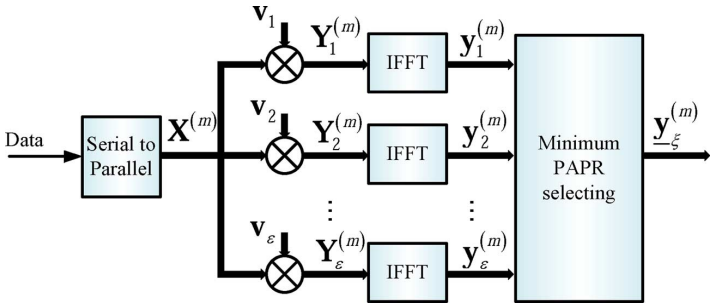


Fig. 3. SLM transmitter block diagram.

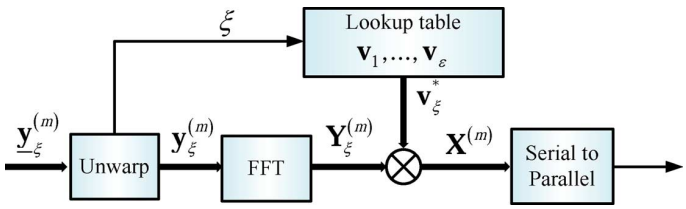


Fig. 4. SLM receiver recovery block diagram.

Each of the cloned $\tilde{\mathbf{X}}^{(m)}$ is multiplied by the appropriate $\mathbf{v}_u$, resulting in the scrambled signal $\mathbf{Y}_u^{(m)}$. An inverse fast Fourier transform (IFFT) procedure is carried out on $\mathbf{Y}_u^{(m)}$, generating $\mathbf{y}_u^{(m)}$. Therefore, the complexity added at the transmitter by the proposed SLM block is $\varepsilon$ IFFT blocks and $\varepsilon$ vector multipliers, each of length $N \cdot L$. After measuring the PAPR value on each of the $\mathbf{y}_u^{(m)}$ set, the $u$ option with the lowest PAPR value is chosen, assigned as $\xi$, and the binary code index of the selected $\mathbf{v}_\xi$ is attached. The transmitted signal is given by: $\underline{\mathbf{y}}_\xi^{(m)} = [\mathbf{y}_\xi^{(m)}, \lceil \log_2(\xi) \rceil]$, and the resulting overhead is $\lceil \log_2(\varepsilon) \rceil$ bits per OFDM symbol, where $\lceil \cdot \rceil$ is the up-round operation.

At the receiver, the SLM-recovery blocks extract the information about the selected $\mathbf{v}_\xi$ from the scrambled data $\mathbf{y}_\xi^{(m)}$. Then, fast Fourier transform (FFT) performed on $\mathbf{y}_\xi^{(m)}$ regenerates $\mathbf{Y}_\xi^{(m)}$. The data is finally recovered after multiplying $\mathbf{Y}_\xi^{(m)}$ by the conjugate selected $\mathbf{v}_\xi$. The amount of PAPR reduction, in SLM, depends on $\varepsilon$, and on the content of the data block [22].

### D. MZM Nonlinear Mitigation Using Digital Compensation

MZM nonlinear mitigation is proposed by artificially increasing the linear region around the null intensity operating point using pre-distortion technique. A basic pre-distortion scheme for the MZM driving voltage can be write in the form:

$$V_a(n) = \frac{2V_\pi}{\pi} \cos^{-1}\left(\frac{x_n}{r_{\max}}\right), \tag{24}$$

where $x_n$ is the OFDM signal, and $r_{\max} = \max\{|x_n|\}$. since $x_n$ is assumed to be real (describe in Section III-A), (24) is also real.

The pre-distortion in (24) artificially increases the linear region of the MZM, but may lead to extremely low driving voltage in the presence of high peak power, as $r_{\max}$ will have very high value. Therefore, we propose to optimize this pre-distortion mechanism by applying a magnification factor $R$, where

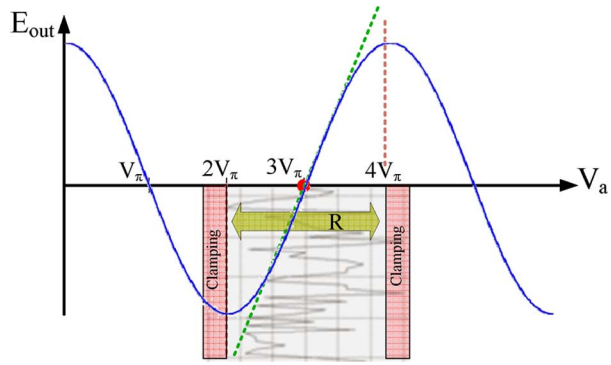


Fig. 5. The MZM output field versus the applied voltage. Illustration of the optimization of MZM pre-distortion function.

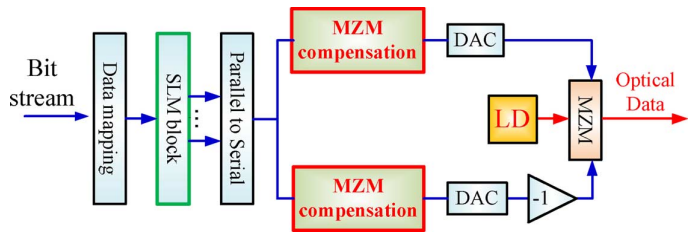


Fig. 6. MZM compensation CO-OFDM transmitter.

$R < r_{\max}$. This magnification factor maximizes the driving signal, while maintaining controlled clipping that optimizes the system performance. A similar approach was introduced by Tang *et al.* [9]. Here, the parameter $R$ effectively serves as an optimized clipping factor, similar to the mechanism being used in power amplifiers in wireless OFDM [1]. In Fig. 5, an illustration of the optimization mechanism is shown. The optimized pre-distortion driving signal can be written as

$$V_a(n) = \begin{cases} 0, & x_n > R \\ \frac{2V_\pi}{\pi} \cos^{-1}\left(\frac{x_n}{R}\right), & |x_n| \le R \\ 2V_\pi, & x_n < (-R). \end{cases} \tag{25}$$

The proposed CO-OFDM transmitter is described in Fig. 6, while the receiver is similar to the standard CO-OFDM, shown in Fig. 2. Compared to the standard CO-OFDM transmitter, shown in Fig. 1, it can be noticed that two main blocks have been added. The first is a well-known PAPR reduction technique block, where SLM is the selected technique. The second added block is the MZM compensation, where it is a DSP block that acts on the applied voltage to the MZM arms, a digital pre-distortion to compensate for the MZM nonlinearity and artificially increase the linear region.

## IV. Analysis of CO-OFDM System

A low pass equivalent (LPE) model of a CO-OFDM communication system is designed in order to analyze the nonlinearity of MZM in the presence of high peak power and to examine techniques to mitigate the nonlinear effect.

At the transmitter side, a data rate of 100 Gbps, with 64-QAM mapping is used to produce an OFDM signal with 128 tones. The selected technique for reducing PAPR is SLM with an order

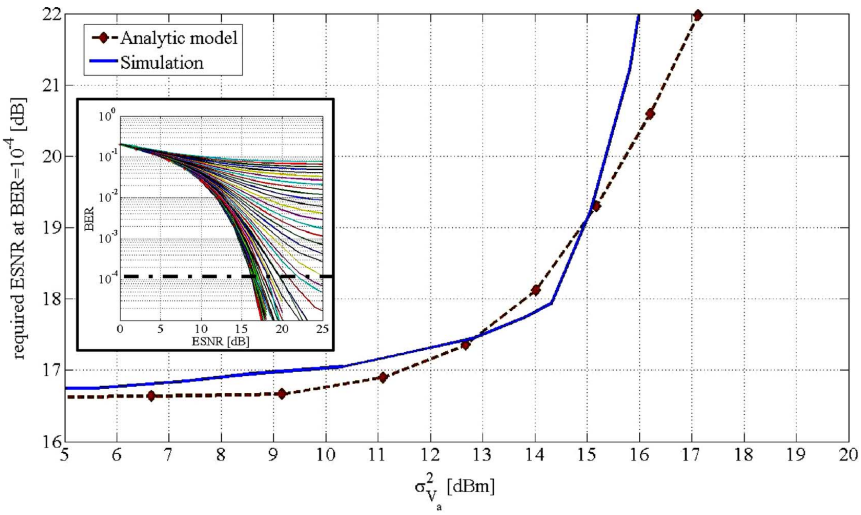


Fig. 7. Comparison with theoretical model of 64-QAM standard CO-OFDM system with 128 tones. Inset: Illustration of BER versus ESNR performance of 64-QAM standard CO-OFDM system with 128 tones.

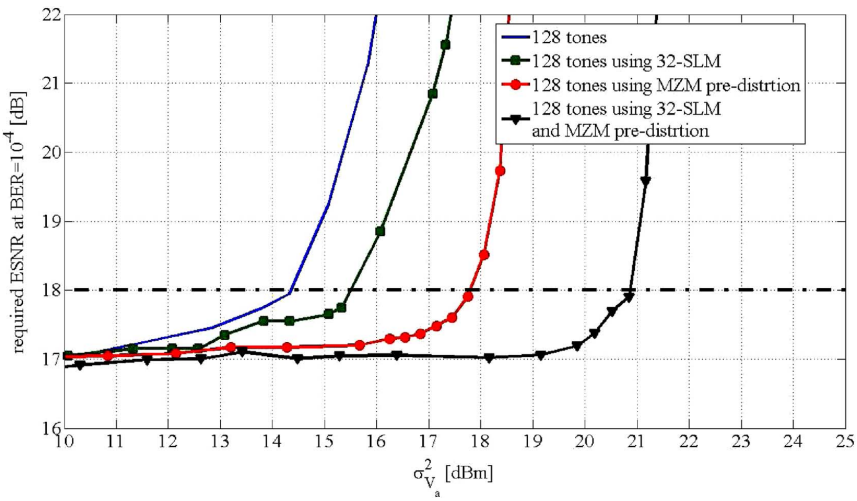


Fig. 8. PAPR mitigation performance of 64-QAM, standard, and improved CO-OFDM system with 128 tones.

of $\varepsilon = \{1, 32\}$, i.e., with or without SLM. At the MZM, $V_\pi$ is normalized, i.e., $V_\pi = 1$.

At the receiver side, the signal is detected by a coherent receiver, which recovers the amplitude and phase of the signal, as described in Section III-A. In turn, the received electrical signal, which is accompanied by electrical additive white Gaussian noise, is sampled. A post-processing unit is assumed to fully compensate for fiber chromatic dispersion (CD) and polarization mode dispersion (PMD), and clock recovery is performed [15], [16]. Finally, the estimated OFDM signal is transformed to the frequency domain and the OFDM symbols are demodulated.

### *A. Standard CO-OFDM System Analysis*

The standard CO-OFDM system, as presented in Section III-A, is analyzed in presence of high peak power, where the applied voltage to the MZM arms is modulated by using a continuous laser with power of $P_{\mathrm{LD}} = 1$ mW; thus only linear fiber effects are introduced.

The 64-QAM standard CO-OFDM with 128 tones is analyzed for various standard deviation values of the applied voltage into the MZM, $\sigma_{V_a}$. While increasing the $\sigma_{V_a}$ values, the BER versus electrical signal to noise ratio (ESNR) performance degrades, due to the MZM nonlinearity, as shown illustratively in the inset of Fig. 7. Each of the plots is associated with a specific $\sigma_{V_a}$ value of the applied voltage into the MZM, $V_a$, as define by (5).

Fig. 7 presents the results of the required ESNR at BER equal to $10^{-4}$, versus variance values of the applied voltage into the MZM, $\sigma^2_{V_a}$, for the case of 128 tones. The dashed curve represents the theoretical analytical results of the 64-QAM CO-OFDM with 128 tones, as described in Section III-B, while the continuous curve represents the simulation results. A good agreement between the simulation results and the analytical model is achieved for $\sigma^2_{V_a}$ values up to 15 dBm. The theoretical model is based on third order polynomial approximation of the MZM cosine behavior, thus it is limited to these values.

In Fig. 8, the two left-hand side curves summarize the SLM performance improvement. The continuous curve is the result for 64-QAM standard CO-OFDM with 128 tones. The "rect-

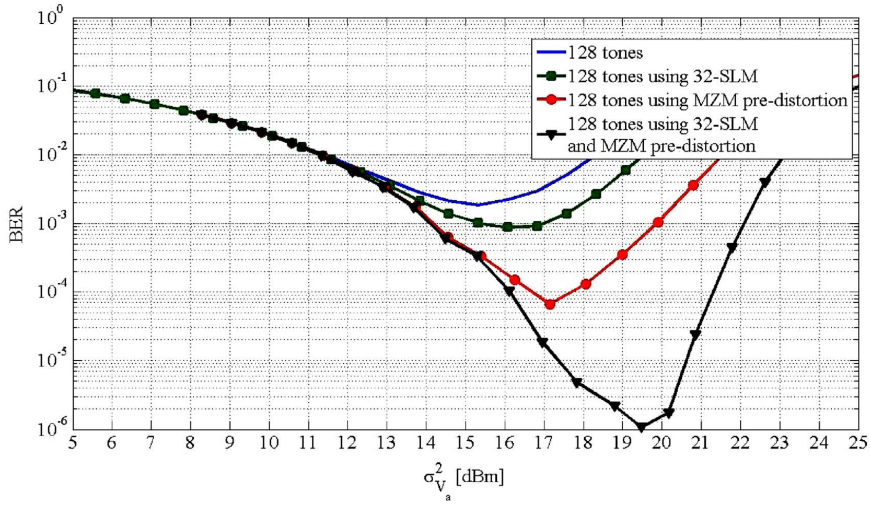


Fig. 9. BER versus $\sigma^2_{V_a}$ performance of 128 tones CO-OFDM system.

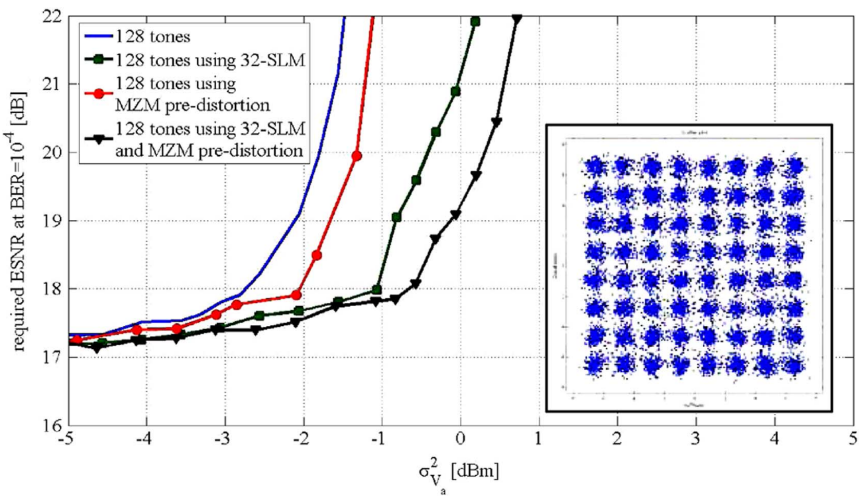


Fig. 10. 64-QAM, 128 tones CO-OFDM system with $P_{\mathrm{LD}} = 13$ mW. Inset: A typical 64-QAM constellation in CO-OFDM system.

angular curve" represents improved results by using 32-SLM. It is observed that by applying SLM technique, greater electrical driving signals can be used, thus greater PAPR values can be applied for the same required ESNR values compared to non-scrambled OFDM signal.

### *B. MZM Compensation CO-OFDM System Analysis*

In this section the proposed CO-OFDM system, as described in Section III-D, is analyzed in the presence of high peak power. As in Section IV-A, the laser output power is of $P_{\mathrm{LD}} = 1$ mW, thus, only the linear fiber effects are introduced.

The 64-QAM improved CO-OFDM system, based on both SLM and the proposed pre-distortion techniques, with 128 tones, is analyzed for various $\sigma_{V_a}$ values with a specific magnification factor $(R)$. Similar to the case of standard CO-OFDM system presented in Section IV-A, while increasing the $\sigma_{V_a}$ values, the BER versus ESNR performance degrades due to MZM nonlinearity.

The simulation results for the 64-QAM improved CO-OFDM system with 128 tones are shown in the "rounds curve" of Fig. 8. As an example, while applying pre-distortion, as described in Section III-D, in the case where the required ESNR is 18 dB at BER equal to $10^{-4}$, an improvement of 3.5 dB in $\sigma^2_{V_a}$ values can be achieved, compared to the standard CO-OFDM case. Furthermore, applying both SLM and pre-distortion techniques leads to a total improvement of 6.5 dB in PAPR tolerance, as presented by the "triangles curve" of Fig. 8. As a result, greater electrical driving signals can be applied to the MZM with no additional PAPR penalty.

The motivation for a greater electrical driving signal can be easily understood when observing the inclusive results shown in Fig. 9. In Fig. 9, the BER versus $\sigma^2_{V_a}$ performance of the 64-QAM CO-OFDM system with 128 tones is shown. At the receiver side the accompanying noise is AWGN with zero mean and $10\ \mathrm{pA}/\sqrt{(\mathrm{Hz})}$.

For a weak signal the system is limited by SNR (left hand side), while strong signals are distorted due to the MZM nonlinearity (right hand side). Significant improvement in the BER results occurs when applying both SLM and pre-distortion, which allows a wide dynamic range of applied voltage to achieve the required BER. This is clearly observed by comparing the continuous curve (no PAPR mitigation techniques involved) with

the "triangles curve" that contains both SLM and pre-distortion effects.

It should be noted that the effective number of bits required by the DAC is six. Lower resolution DAC will introduced performance degradation. Similar results were obtained by [9].

### C. CO-OFDM System in Presence of Nonlinear Fiber Effects Analysis

In this section the standard and the proposed CO-OFDM systems are analyzed for the case of high launched power into the fiber. The system parameters include: 64-QAM CO-OFDM system with 128 tones, $P_{\mathrm{LD}} = 13$ mW, and fiber length of $L = 100$ km. These parameter values represent an example of a metropolitan network scenario with significant transmitted optical power. For this high power case, the nonlinear fiber effect, i.e., SPM is pronounced.

A summary of the simulation results is shown in Fig. 10. As can be observed, for the CO-OFDM system with $P_{\mathrm{LD}} = 13$ mW, an improvement in the system performance can also be achieved by using the SLM technique. However, the effectiveness of the pre-distortion is less pronounced as the SPM nonlinear effect dominates, compared to the MZM distortion.

Also evident from the inset is that the constellation distortion is isotropic and uniform per symbol, as opposed to single carrier non-isotropic symbol distortion associated with SPM [23]. This can be explained by the fact that in the proposed CO-OFDM system each tone experiences different SPM-related phase shift, thus the total constellation distortion is averaged out. Similar results of SPM distortion in the OFDM system were observed in [5].

## V. Conclusion

PAPR tolerance in the CO-OFDM system is analyzed. MZM pre-distortion and SLM mitigation techniques are introduced. Inclusive performance analysis reveals an increased tolerance to applied electrical driving signals and thus increased tolerance to PAPR, while keeping the same performance requirement by means of required ESNR at fixed BER. This technique enables flexibility in CO-OFDM design and optimization by means of number of tones, PAPR, and resulting tradeoff between required ESNR versus bandwidth efficiency.

In addition, preliminary theoretical modelling for the MZM nonlinear distortion is presented. A good agreement between simulation results to analytical model is achieved for up to medium signal intensity, as the theoretical model is based on third order polynomial approximation of the MZM cosine behavior.

## References


[1] L. Hanzo, M. Münster, B. J. Choi, and T. Keller, *OFDM and MC-CDMA for Broadband Multi-User Communications, WLANs and Broadcasting*. New York: Wiley, 2003, pp. 47–48.

[2] W. Shieh and I. Djordjevic, *Orthogonal Frequency Division Multiplexing for Optical Communication*. Amsterdam, The Netherlands: Elsevier, 2010, pp. 38–39.

[3] S. H. Han and J. H. Lee, "An overview of peak to average power ratio reduction techniques for multicarrier transmission," *Wireless Commun.* , pp. 56–65, Apr. 2005.

[4] B. Goebel, S. Hellerbrand, N. Haufe, and N. Hanik, "PAPR reduction techniques for coherent optical OFDM transmission," in *Proc. ICTON 2009*, Jul. 2009.

[5] A. J. Lowery, "Fiber nonlinearity pre- and post-compensation for long-haul optical links using OFDM," *Opt. Express*, vol. 15, no. 20, Oct. 2007.

[6] X. Liu and R. W. Tkach, "Joint SPM compensation for inline-dispersion-compensated 112-Gb/s PDM-OFDM transmission," in *Proc. OFC/NFOEC*, San Diego, Mar. 2010, paper OThO5.

[7] R. I. Kelly *et al.*, "Electronic dispersion compensation by signal predistortion using digital processing and a dual-drive Mach–Zehnder modulator," *IEEE Photon. Technol. Lett.*, vol. 17, no. 3, pp. 714–716, Mar. 2005.

[8] C. Weber *et al.*, "Electronic precompensation of intrachannel nonlinearities at 40 Gb/s," *IEEE Photon. Technol. Lett.*, vol. 18, no. 16, pp. 1759–1761, Aug. 2006.

[9] Y. Tang, K. P. Ho, and W. Shieh, "Coherent optical OFDM transmitter design employing predistortion," *IEEE Photon. Technol. Lett.*, vol. 20, no. 11, pp. 954–956, Jun. 2008.

[10] J. Tellado, *Multicarrier Modulation With Low PAR: Applications to DSL and Wireless*. Dordrecht, The Netherlands: Kluwer, 2000, p. 18.

[11] C. Tellambura, "Computation of the continuous–time PAR of an OFDM signal with BPSK subcarriers," *IEEE Commun. Lett.*, vol. 5, no. 5, pp. 185–187, May 2001.

[12] G. P. Agrawal, *Nonlinear Fiber Optics*, 4th ed. Amsterdam, The Netherlands: Elsevier, 2007, pp. 40–46.

[13] G. P. Agrawal, *Fiber-Optic Communication Systems*, 3rd ed. New York: Wiley, 2002.

[14] E. Ip, A. P. T. Lau, D. J. F. Barros, and J. M. Kahn, "Coherent detection in optical fiber systems," *Opt. Express*, vol. 16, no. 2, pp. 753–791, Jan. 2008.

[15] E. Ip and J. M. Kahn, "Digital equalization of chromatic dispersion and polarization mode dispersion," *J. Lightw. Technol.*, vol. 25, no. 8, pp. 2033–2043, Aug. 2007.

[16] A. Gorshtein, D. Sadot, G. Katz, and O. Levy, "Coherent CD equalization for 111 Gbps DP-QPSK with one sample per symbol based on anti-aliasing filtering and MLSE," in *Proc. OFC/NFOEC*, San Diego, Mar. 2010, paper OThT2.

[17] G. L. Li and P. K. L. Yu, "Optical intensity modulators for digital and analog applications," *J. Lightw. Technol.*, vol. 21, no. 9, pp. 2010–2029, Sep. 2003.

[18] V. A. Bohara and S. H. Ting, "Theoretical analysis of OFDM signals in nonlinear polynomial models," in *Proc. ICICS*, Singapore, Dec. 2007.

[19] J. G. Proakis, *Digital Communications*. New York: McGraw-Hill, 1995.

[20] H. Ochiai and H. Imai, "On the distribution of the peak-to-average power ratio in OFDM signals," *IEEE Trans. Commun.*, vol. 49, no. 2, pp. 282–289, Feb. 2001.

[21] K. Cho and D. Yoon, "On the general BER expression of one- and two-dimensional amplitude modulations," *IEEE Trans. Commun.*, vol. 50, no. 7, pp. 1074–1080, Jul. 2002.

[22] S. H. Müller, R. W. Bäuml, R. F. H. Fischer, and J. B. Huber, "OFDM with reduced peak-to-average power ratio by multiple signal representation," *Ann. Telecommun.*, vol. 52, no. 1–2, pp. 58–67, 1997.

[23] K. P. Ho and J. M. Khan, "Electronic compensation technique to mitigate nonlinear phase noise," *J. Lightw. Technol.*, vol. 22, pp. 779–783, 2004.



**Yanir London** received the B.Sc. degree (*summa cum laude*) in electrical engineering from the Holon Academic Institute of Technology, Holon, Israel, in 2004, and the M.Sc. degree in electrical engineering from the Ben Gurion University of the Negev, Beer Sheva, Israel, where he is currently working toward the Ph.D. degree in electrical engineering.

His research interest includes OFDM in optical communication application.

**Prof. Dan Sadot** received the B.Sc., M.Sc., and Ph.D. *(summa cum laude)* degrees from the Ben Gurion University of the Negev, Beer Sheva, Israel, in 1988, 1990, and 1994, respectively, all in electrical and computer engineering.

During 1994–1995, he was a Post-Doctorate associate at the Department of Electrical Engineering of Stanford University. His Ph.D. studies were supported by the Clore scholarship, and his post-doctorate was supported by both the Fulbright and the Rothchild scholarships. Currently, he is Chairman of the Electrical and Computers Engineering Department at Ben Gurion University.